Acta Crystallographica Section D
Biological Crystallography
ISSN 0907-4449

Novel structural features in the GMC family of oxidoreductases revealed by the crystal structure of fungal aryl-alcohol oxidase

Israel S. Fernández, Francisco J. Ruíz-Dueñas, Elena Santillana, Patricia Ferreira,‡ María Jesús Martínez, Ángel T. Martínez and Antonio Romero*

Centro de Investigaciones Biológicas, CSIC, Ramiro de Maeztu 9, E-28040 Madrid, Spain

‡ Present address: Departamento de Bioquímica y Biología Molecular y Celular, Facultad de Ciencias and Instituto de Biocomputación y Física de Sistemas Complejos, Universidad de Zaragoza, E-50009 Zaragoza, Spain.

Correspondence e-mail: romero@cib.csic.es

Received 9 July 2009
Accepted 4 September 2009

PDB Reference: aryl-alcohol oxidase, 3fim, r3fimsf.

Lignin biodegradation, a key step in carbon recycling in land ecosystems, is carried out by white-rot fungi through an H_2O_2-dependent process defined as enzymatic combustion. *Pleurotus eryngii* is a selective lignin-degrading fungus that produces H_2O_2 during redox cycling of *p*-anisylic compounds involving the secreted flavoenzyme aryl-alcohol oxidase (AAO). Here, the 2.4 Å resolution X-ray crystal structure of this oxidoreductase, which catalyzes dehydrogenation reactions on various primary polyunsaturated alcohols, yielding the corresponding aldehydes, is reported. The AAO crystal structure was solved by single-wavelength anomalous diffraction of a selenomethionine derivative obtained by *Escherichia coli* expression and *in vitro* folding. This monomeric enzyme is composed of two domains, the overall folding of which places it into the GMC (glucose–methanol–choline oxidase) oxidoreductase family, and a noncovalently bound FAD cofactor. However, two additional structural elements exist in the surroundings of its active site that modulate the access of substrates; these are absent in the structure of the model GMC oxidoreductase glucose oxidase. The folding of these novel elements gives rise to a funnel-like hydrophobic channel that connects the solvent region to the buried active-site cavity of AAO. This putative active-site cavity is located in front of the *re* side of the FAD isoalloxazine ring and near two histidines (His502 and His546) that could contribute to alcohol activation as catalytic bases. Moreover, three aromatic side chains from two phenylalanines (Phe397 and Phe502) and one tyrosine (Tyr92) at the inner region of the channel form an aromatic gate that may regulate the access of the enzyme substrates to the active site as well as contribute to the recognition of the alcohols that can effectively be oxidized by AAO.

1. Introduction

Lignin is a heterogeneous polymer made up of phenylpropanoid units with diverse methoxylation patterns and different interunit linkages (Ralph *et al.*, 2004; Martinez *et al.*, 2008). This complex macromolecule is one of the main components of wood and other lignocellulose materials, together with cellulose and hemicellulose (Higuchi, 1997). Lignin confers physical resistance to these materials by acting as cement between cellulosic fibres and forming an amorphous matrix in the wood secondary wall, in which the cellulose fibrils are embedded. The lignin polymer is highly resistant to chemical or biological degradation owing to its aromatic nature and complex three-dimensional structure. The molecular characteristics of lignin, with its random and highly hydrophobic chemical structure, as well as its high molecular mass, constrain the pattern of degradation followed by lignin-degrading

organisms. White-rot basidiomycetes are the only organisms that can fully degrade lignin, which is a key step in recycling the carbon photosynthetically fixed in wood. The ligninolytic machinery of white-rot fungi is integrated by a set of secreted oxidative enzymes that degrade lignin in a nonspecific H_2O_2-dependent process defined as 'enzymatic combustion' (Kirk & Farrell, 1987).

The absolute dependence of the lignin-degrading system on the continuous supply of H_2O_2 is a consequence of the high redox potential needed for the oxidation of the nonphenolic components of the lignin polymer (Martinez *et al.*, 2005). A collection of H_2O_2-dependent peroxidases, the so-called lignin peroxidases, manganese peroxidases and versatile peroxidases (Ruiz-Dueñas *et al.*, 2009), together with other oxidative enzymes secreted by the white-rot fungi (*e.g.* laccases; Baldrian & Valaskova, 2008) initiate the attack on lignin, which finally results in the complete depolymerization and degradation of the recalcitrant polymer. Another role for H_2O_2 in wood biodegradation has also been suggested owing to its ability to generate hydroxyl radicals (OH·) that might initiate the attack on lignocellulose when the enzymes cannot penetrate the plant cell wall (Evans *et al.*, 1994).

Our understanding of the natural process of lignin biodegradation is far from complete. In addition to the implication of this biodegradation process in the natural recycling of carbon, the potential of white-rot fungi and their enzymes in environmentally friendly biotechnological processes is being explored. These include a variety of industrial applications such as the manufacture of paper, the production of bioethanol and the biodegradation of pollutants.

Pleurotus eryngii is a basidiomycete whose ligninolytic system has been widely characterized as a consequence of its ability to selectively remove lignin (Martinez *et al.*, 2005). This system involves manganese peroxidases (Camarero *et al.*, 1994), versatile peroxidases (Ruiz-Dueñas *et al.*, 2009), laccases (Muñoz *et al.*, 1997) and a specific H_2O_2-generating enzyme called aryl-alcohol oxidase (AAO; Guillen *et al.*, 1992). AAO is secreted by *P. eryngii* as a monomeric glycoflavoprotein with a molecular mass of 69.1 kDa that uses dissociable FAD as a cofactor. Primary structure analysis of AAO revealed that it belongs to the GMC (glucose–methanol–choline) oxidoreductase family of flavoproteins (Cavener, 1992) that contain several consensus sequences, including a N-terminal conserved $\beta\alpha\beta$ dinucleotide-binding motif (DBM) that is involved in FAD binding (Varela *et al.*, 2000).

P. eryngii AAO displays remarkable substrate specificity (Ferreira *et al.*, 2005, 2006) as it can catalyze dehydrogenation reactions on a wide range of primary unsaturated alcohols with the production of H_2O_2. In the reductive half-reaction, AAO catalyzes the oxidation of alcohol substrates to yield the corresponding aldehydes, while the FAD is reduced to $FADH_2$. During the oxidative half-reaction, the flavin is reoxidized by O_2 and H_2O_2 is produced. Kinetic studies showed that *p*-anisyl alcohol is the preferred substrate of AAO, although a set of related chemical compounds can also be efficiently oxidized by the enzyme, such as benzyl, naphthyl or cinnamyl alcohols, together with aliphatic polyunsaturated alcohols and halogenated benzyl alcohols; the enzyme also displays residual activity on some aromatic aldehydes (Ferreira *et al.*, 2006). It is noteworthy that *p*-anisaldehyde, the product of AAO oxidation when it uses its preferred substrate, is the most abundant extracellular metabolite in *P. eryngii* cultures (Gutierrez *et al.*, 1994) and that a continuous supply of H_2O_2 is obtained by the redox cycling of this compound involving AAO and mycelium-associated dehydrogenases (Guillen & Evans, 1994).

The gene coding for the AAO protein of *P. eryngii* has been cloned (Varela *et al.*, 1999) and a prokaryotic heterologous expression system has been developed to obtain fully active nonglycosylated AAO for biochemical and structural studies (Ruiz-Dueñas *et al.*, 2006). This has facilitated the current studies into the mode of action of *P. eryngii* AAO (Ferreira *et al.*, 2006). Notably, there is no evidence for the stabilization of a semiquinone anionic intermediate during reduction to the flavin hydroquinone form, as produced by most oxidases. Thus, an electrophilic attack mechanism has been proposed for alcohol substrate oxidation that is similar to that proposed for glucose oxidase (GOX), in which one of two histidine residues located on the *re* face of the flavin ring near its N^5 atom would act as a general base. Through substrate alkoxide formation, the histidine residue could contribute to hydride transfer to FAD in the reductive half-reaction.

Here, we present the three-dimensional structure of AAO from *P. eryngii* solved by X-ray crystallography using experimental phasing procedures from a selenium derivative. The atomic structure of AAO exhibits novel features that were not expected from previous primary-structure analysis or from molecular modelling (Varela *et al.*, 2000; Ferreira *et al.*, 2006). Standing out among these novel features is the presence of two structural elements that form a channel into an inner cavity adjacent to the isoalloxazine ring of the FAD cofactor and two conserved histidines, where it is probable that catalysis takes place. It is proposed that access to this inner cavity is regulated by three aromatic residues that block or permit traffic through the channel. This information will assist in the rationalization of previous kinetic and biochemical studies on the generation of H_2O_2 during the oxidation of aromatic alcohols by the model ligninolytic fungus *P. eryngii*.

2. Materials and methods

2.1. AAO expression, purification and crystallization

The expression in *Escherichia coli*, *in vitro* refolding and characterization of recombinant *P. eryngii* AAO (GenBank AF064069) have been described elsewhere (Ruiz-Dueñas *et al.*, 2006). SeAAO was obtained following standard protocols without using auxotroph strains (Van Duyne *et al.*, 1993). UV–visible spectra of AAO were recorded in 10 m*M* sodium phosphate pH 5.5 using a Hewlett Packard (Loveland, Colorado, USA) 8453 spectrophotometer to check the correct FAD binding and enzyme conformation and to calculate the enzyme concentration. The molecular masses of AAO and SeAAO were estimated by MALDI–TOF mass spectrometry (Bruker) to check the incorporation of selenomethionine

residues. Crystallization was achieved by the sitting-drop vapour-diffusion method from a protein solution at 6 mg ml^{-1} in 150 m*M* NaCl and 0.1 *M* NaK_2PO_4 pH 7.0. The best crystals of native AAO and SeAAO were obtained after two weeks at 295 K by mixing equal volumes (1 µl) of protein and reservoir solutions. The latter solution consisted of 1 *M* Li_2SO_4, 0.1 *M* bis-Tris propane pH 7.4.

2.2. X-ray data collection

For cryoprotection, crystals were stabilized in 15%(*v*/*v*) glycerol, 1.5 *M* Li_2SO_4, 100 m*M* bis-Tris propane pH 7.4 and flash-frozen by immersion in liquid N_2. Native AAO crystals diffracted to 2.4 Å resolution on beamline BM16 at the ESRF, Grenoble, France. Two-wavelength MAD data sets were collected using SeAAO crystals at the BW7A station at DESY, Hamburg, Germany, although only the Se *K*-edge absorption peak data to 2.5 Å resolution were used to solve the structure. Images were auto-indexed and integrated with *MOSFLM* (Leslie, 2006) and scaling and merging was performed with *SCALA* (Evans, 2006) from the *CCP*4 suite (Collaborative Computational Project, Number 4, 1994). The systematic absences and symmetry were consistent with space group $P6_422$ or $P6_222$.

2.3. SAD phasing and refinement

SAD phases were derived from an SeAAO crystal using the *SHELX* program (Sheldrick, 2008) as implemented in the *HKL2MAP* interface (Pape & Schneider, 2004). Patterson-seeded dual-space direct methods were used for a heavy-atom search as implemented in *SHELXD* (Sheldrick, 2008). Six of the nine Se atoms were clearly located, from which phases were derived and density-modified using *SHELXE* (Sheldrick, 2008). Well defined continuous electron-density maps gave a clear representation of the protein molecule from the calculated phases in space group $P6_422$. Further statistical density modification was performed as implemented in *PIRATE* (Cowtan & Zhang, 1999) before the phases were exported to *ARP*/*wARP* (Langer *et al.*, 2008) to build the initial model. A single round of *ARP*/*wARP* was sufficient to almost completely build the polypeptide-chain amino acids 2–560, which corresponded to more than 95% of the AAO protein sequence. A first restrained refinement was performed with this initial model and the derivative data as implemented in *REFMAC* (Murshudov *et al.*, 1997), yielding an initial *R* and $R_{\rm free}$ of 26.5% and 31.2%, respectively. Visual inspection and model rebuilding were carried out with *Coot* (Emsley & Cowtan, 2004). Additional continuous density was observed within the protein volume compatible with the FAD cofactor. The new *ARP*/*wARP* building module (Langer *et al.*, 2008) was used to position the cofactor in this additional electron density using a PDB file and a molecular restraint file for FAD generated using the *PRODRG* web server (van Aalten *et al.*, 1996). Another round of restrained refinement was performed including the FAD molecule before the model was refined and rebuilt against the high-resolution data from the native crystal. TLS refinement was employed at the later stages of the refinement as implemented in *REFMAC* (Winn *et al.*, 2003). Four TLS groups were defined: one for each of the two extra structural elements, one for the rest of the protein and one for the cofactor. The final step of the refinement process involved the addition of ordered solvent molecules to the model using the 'find water' option of *Coot*.

Table 1
Data-collection, phasing and refinement statistics.

Values in parentheses are for the highest resolution shell.

	SeAAO	AAO
Data collection and phasing		
Space group	$P6_422$	$P6_422$
Unit-cell parameters	$a = b = 179.09$, $c = 159.31$, $\alpha = \beta = 90.0$, $\gamma = 120.0$	$a = b = 180.23$, $c = 160.40$, $\alpha = \beta = 90.0$, $\gamma = 120.0$
Wavelength (Å)	0.978	0.85
Resolution (Å)	19.90–2.55 (2.40–2.55)	49.51–2.39 (2.25–2.39)
Reflections	49228	56141
Completeness (%)	97.3 (81.8)	97.07 (88.8)
Multiplicity	21.9 (9.4)	15.0 (7.6)
Mean $I/\sigma(I)$	30.8 (8.0)	21.6 (4.0)
$R_{\rm merge}$	9.1 (51.3)	10.2 (46.4)
Anomalous completeness	97.1 (81.0)	
Anomalous multiplicity	11.5 (10)	
$R_{\rm Cullis}$	0.74	
Phasing power	2.1	
FOM	0.82	
Se sites	6	
Refinement statistics		
$R_{\rm work}$ (%)		17.33
$R_{\rm free}$ (%)		20.64
Average *B* factor (Å^2)		35.68
No. of atoms		
Protein		4296
FAD		53
Solvent		225
Total		4574
R.m.s.d.		
Bond distances (Å)		0.022
Bond angles (°)		1.961

Validation of the final refined structure was performed with *MolProbity* (Davis *et al.*, 2007) and *PROCHECK* (Laskowski *et al.*, 1993). Key statistics of the quality of the model, reflection data and structure refinement are presented in Table 1. Cavities and accessibility surfaces were calculated with *CAVER* (Petrek *et al.*, 2006). *CHIMERA* (Pettersen *et al.*, 2004) and *PyMOL* (DeLano, 2002) were used to generate illustrations and *ESPript* (Gouet *et al.*, 1999) was used to generate the sequence-alignment figure.

3. Results and discussion

3.1. X-ray crystal structure and overall folding

P. eryngii AAO and its selenium derivative (SeAAO) were expressed in *E. coli* as inclusion bodies and activated *in vitro*. Correct folding and cofactor incorporation were confirmed by characteristic electronic absorption spectra (Guillen *et al.*, 1992; Ruiz-Dueñas *et al.*, 2006); matrix-assisted laser desorption/ionization–time of flight (MALDI–TOF) mass spectrometry confirmed the selenium labelling of the

methionine residues. AAO was crystallized in space group $P6_422$, with one molecule per asymmetric unit. The structure was solved by single-wavelength anomalous diffraction (SAD) and refined against native data to 2.4 Å resolution. Clear electron densities were observed for all the residues present in the cloned construct except for the first two residues. The overall shape of the molecule is that of an elongated 'cylinder' crowned by a 'cap'. The length of the cylinder plus the cap is approximately 75 Å and its diameter is about 40 Å, whereas the maximum width of the cap is around 60 Å (Fig. 1*b*). Based on the topology of the solved structure and on their distinct functional roles, two domains could be defined in AAO (Fig. 1): a substrate-binding domain that matches the previously defined cap and an FAD-binding domain that corresponds to the cylinder region.

The FAD-binding domain is formed by three β-sheets that intercollate adjoining β-strands in the primary sequence, which were named following the GOX nomenclature (Varela *et al.*, 2000; Hecht *et al.*, 1993). The whole domain is a novel variation of the glutathione reductase fold, into which a subset of flavoproteins have already been classified (Dym & Eisenberg, 2001). The FAD-binding domain consists of a central five-stranded parallel β-sheet (Fig. 1, sheet *A*) surrounded by three α-helices and an additional crossover connection comprised of a three-stranded antiparallel β-sheet (sheet *B*). At the same time, this additional three-stranded β-sheet is connected to another β-sheet motif of two antiparallel β-strands (sheet *B*′) which is absent from the GOX crystal structure (Hecht *et al.*, 1993). The central core of the substrate-binding domain is formed by a six-stranded antiparallel β-sheet (sheet *C*) flanked by two long α-helices similar to the substrate-binding domain of vanillyl-alcohol oxidase (VAO; Mattevi *et al.*, 1997) or *p*-cresol methylhydroxylase (Mathews *et al.*, 1991). This central core is laterally decorated by two groups of two α-helices that form the widest portion of the cap.

Two connections between the substrate-binding domain and the FAD-binding domain are clearly seen in the AAO structure. One involves three long nonstructured segments that spread out from one domain to the other (Fig. 1*b*, red) and the other involves two extended two-stranded parallel β-sheets situated at the interface between the two domains (Fig. 1, sheets *D* and *E*).

3.2. Structural comparison with other GMC oxidoreductases

A structural similarity search was carried out using the *DALI* web server (Holm & Sander, 1996) with the solved structure of AAO as the probe. The highest scores corresponded to choline oxidase (CHOX; *Z* score 47.3) from *Arthrobacter globiformis* (Quaye *et al.*, 2008) and GOX (*Z* score 42.3) from the ascomycetous fungus *Aspergillus niger* (Hecht *et al.*, 1993). Low matching scores were obtained for other related flavoenzymes such as pyranose-2-oxidase (Bannwarth *et al.*, 2004) and the flavin domain of cellobiose dehydrogenase (Hallberg *et al.*, 2002) from white-rot basidiomycetes and bacterial cholesterol oxidase (Lario *et al.*, 2003), all three of which are from the GMC oxidoreductase family.

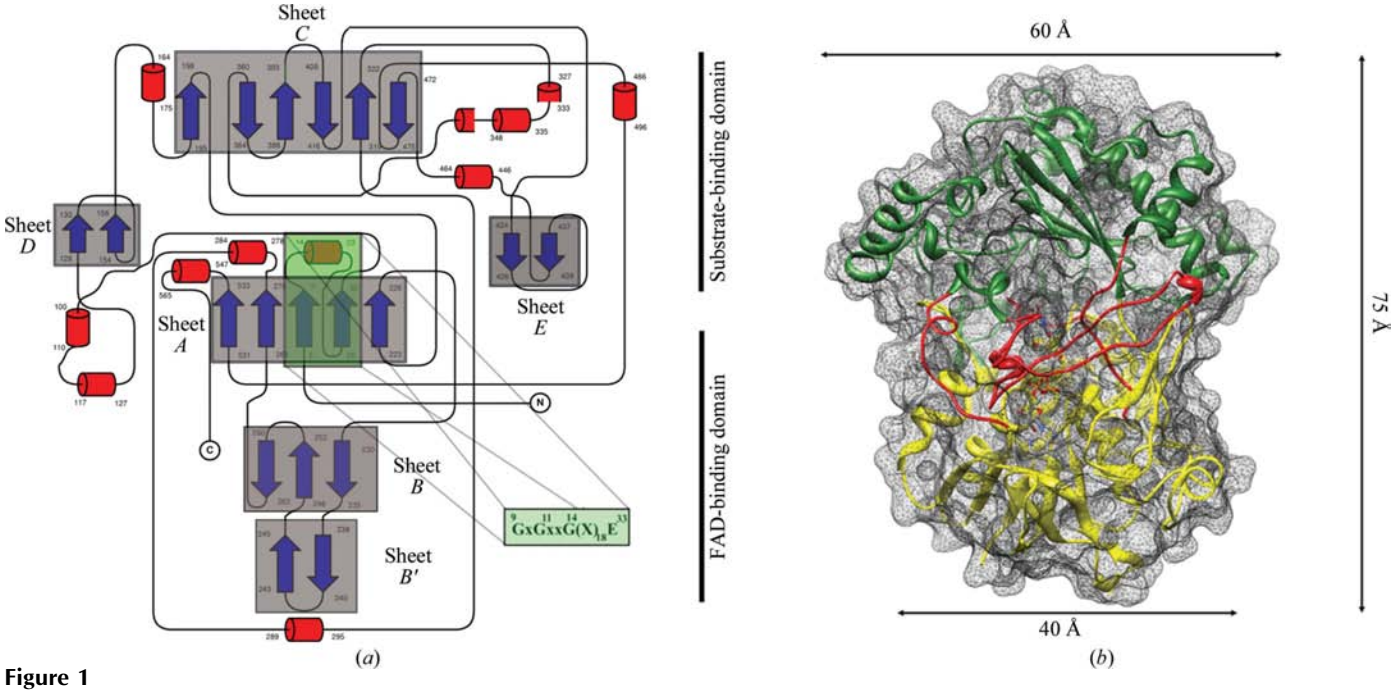

Figure 1
The crystal structure of *P. eryngii* AAO. (*a*) Secondary-structure assignment as implemented in *CHIMERA* (Pettersen *et al.*, 2004). β-Strands are depicted as blue arrows, whereas α-helices are depicted as red cylinders. A green box marks the DBM sequence conserved in the primary structure of AAO. (*b*) Three-dimensional structure of AAO derived from crystallographic data. The apoenzyme is represented as a ribbon diagram inserted in the transparent molecular surface. The substrate-binding domain (cap) is represented in green and the FAD-binding domain in yellow (cylinder). The cofactor (FAD) is represented as sticks coloured according to the atom type. The long unstructured elements that connect the cap and cylinder domains are represented in red in the ribbon diagram.

The superimposition of AAO C^{α} atoms with those of CHOX yielded a root-mean-square deviation (r.m.s.d.) of 2.56 Å, whereas superimposing GOX gave an r.m.s.d. of 4.70 Å. In a structure-based sequence alignment (Fig. 2) the three structures share a common topological domain distribution based on the cylinder–cap scheme described previously. Major differences were found in the N-terminal region (N-T), with AAO having the shortest extension. In contrast, GOX exhibited a long nonstructured N-terminal tail that wraps around the bottom part of the FAD-binding domain, while the N-terminal extension of CHOX was of intermediate length. GOX shows an helical insertion formed by 50 residues (marked *** in Fig. 2) in a different region of the molecule that is lacking in CHOX and that is reduced to only 13 residues, including a unique helix, in AAO.

The structure of AAO displayed another peculiarity at the interface of the two protein domains above the FAD isoalloxazine ring. In GOX access to the active site is wide and unblocked, whereas in CHOX and especially in AAO access is hampered by the presence of additional structural elements (Fig. 2). A 17-amino-acid insertion is present in CHOX (marked ** in Fig. 2) when compared with the GOX primary structure which extends from the antiparallel β-sheet that forms the central core of the substrate-binding domain towards the FAD-binding domain. This feature is more pronounced in AAO, where in addition to a 14-amino-acid insertion (marked ** in Fig. 2) at the same site as in CHOX there is also a further 30-residue insertion (marked * in Fig. 2) that folds as a group of three α-helices protruding from the antiparallel β-sheet (sheet *C*) of the substrate-binding domain. Together, these two insertions generate a platform above the active site of AAO that notably restricts access to the isoalloxazine ring of FAD (Fig. 2*b*).

3.3. The environment of the FAD cofactor

After the first round of structural refinement, the electron density unambiguously localized the cofactor and, as expected from previous studies (Ruiz-Dueñas *et al.*, 2006), only noncovalent interactions were found between FAD and the apoenzyme. The isoalloxazine moiety of FAD in the AAO structure is not planar. An OMIT map calculated without the FAD molecule and the neighbouring residues clearly shows the planar distortion of this structure, generating a butterfly bend along the N^5–N^{10} axis of the isoalloxazine ring. Flavin

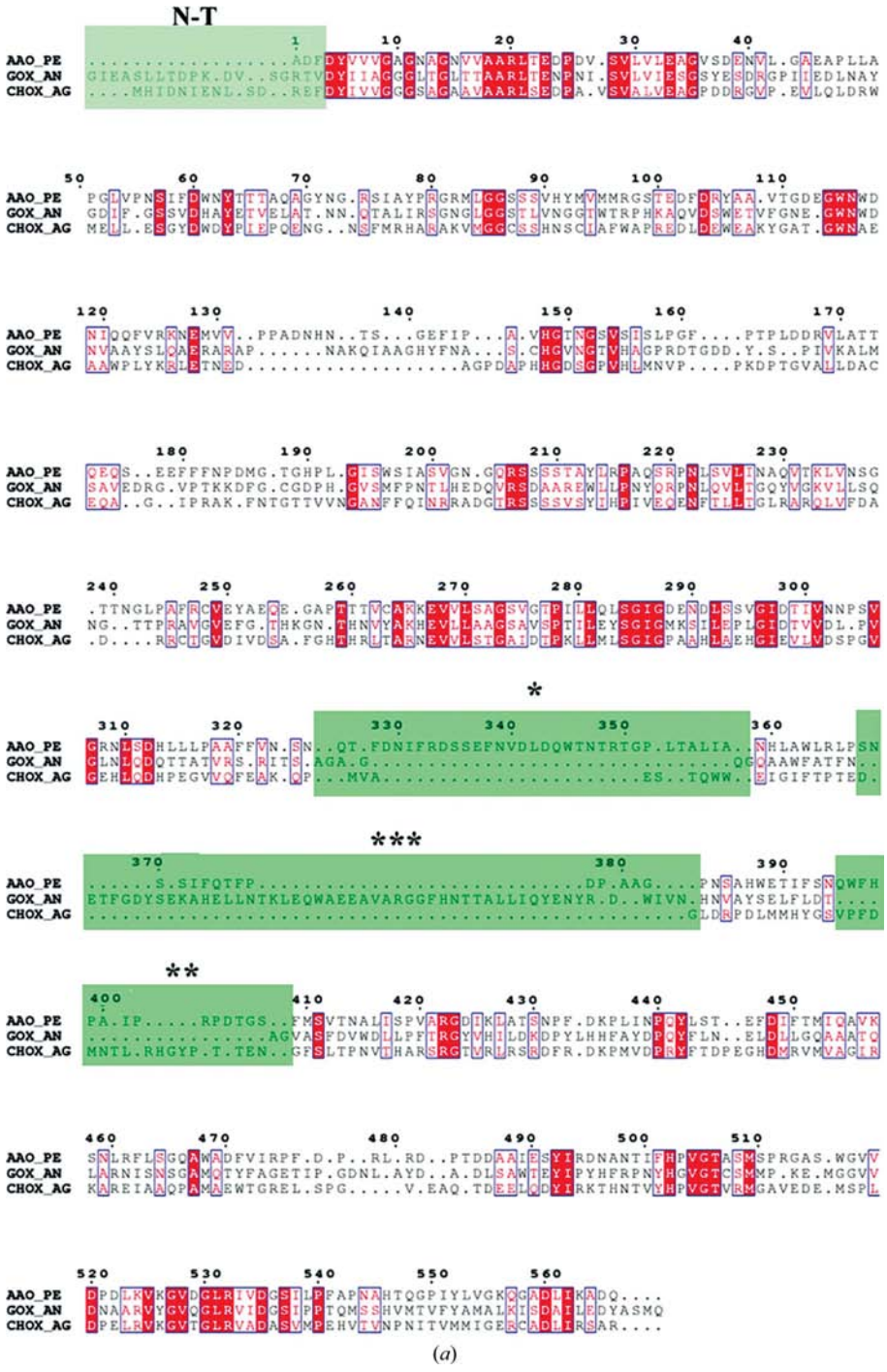

Figure 2
Structure-based sequence alignment of AAO, CHOX and GOX. (*a*) A *DALI* (Holm & Sander, 1996) web server search performed with the three-dimensional structure of AAO yielded CHOX from *A. globiformis* (Quaye *et al.*, 2008) and GOX from *A. niger* (Hecht *et al.*, 1993) as the most similar structures. Red boxes show invariant conserved residues. The main primary structural differences between the three enzymes (labelled *, **, *** and N-T) are marked as green boxes.

distortions have also been described for other flavooxidases and have been associated with redox potential and substrate binding (Mattevi, 2006; Lyubimov *et al.*, 2007); some distortions can also be a consequence of FAD reduction by radiation-generated electrons (Carugo & Carugo, 2005).

The FAD molecule interacts with the protein through a network of hydrogen bonds, predominantly involving the main-chain NH and CO groups of residues located at the N-terminus (Fig. 3) plus several water molecules. The FAD molecule adopts an extended conformation, with the adenine and the isoalloxazine moieties distal to each other and aligned with the vertical axis of the cylinder that constitutes the FAD-binding domain. A consensus N-terminal signature for DBM is found in the primary structure of AAO (Fig. 1*a*, green). This signature is part of the central core of the FAD-binding domain and it adopts a $\beta\alpha\beta$ fold in which the most prominent residues implicated in the stabilization of the cofactor are located. In particular, a number of AAO residues implicated in the interaction with FAD are located in the loop connecting the first β-strand and the α-helix of the DBM signature motif. Direct hydrogen bonds are established between the pyrophosphate moiety of FAD and the main-chain atoms of this loop, as well as between the O2′ and O3′ hydroxyls of the ribose moiety of FAD and the carboxylic group of Glu33 (Figs. 3*a* and 3*b*). The N-terminus of the α-helix that pertains to the DBM motif is oriented towards the pyrophosphate moiety of FAD for charge compensation.

Interestingly, the isoalloxazine moiety of the FAD molecule is deeply buried inside the apoenzyme, with direct access to bulk solvent limited to a small opening. Therefore, the N^5 atom of the isoalloxazine ring directly involved in flavoenzyme catalysis is not directly accessible from the solvent in the structure presented, being located in a relatively small internal cavity (with an estimated volume of 165 Å^3). Buried active sites have also been described for other flavooxidases, such as cholesterol oxidase (Chen *et al.*, 2008) and VAO (Mattevi *et al.*, 1997). Access of the substrates to these shielded active sites has been proposed to be mediated by hydrophobic channels, especially in those enzymes with one or more gases as substrates, as in the case of oxidases (Chen *et al.*, 2008). A detailed analysis of the AAO structure revealed a funnel-like channel that connects the solvent with the surroundings of the N^5 atom of the isoalloxazine ring of FAD (Fig. 4). This channel

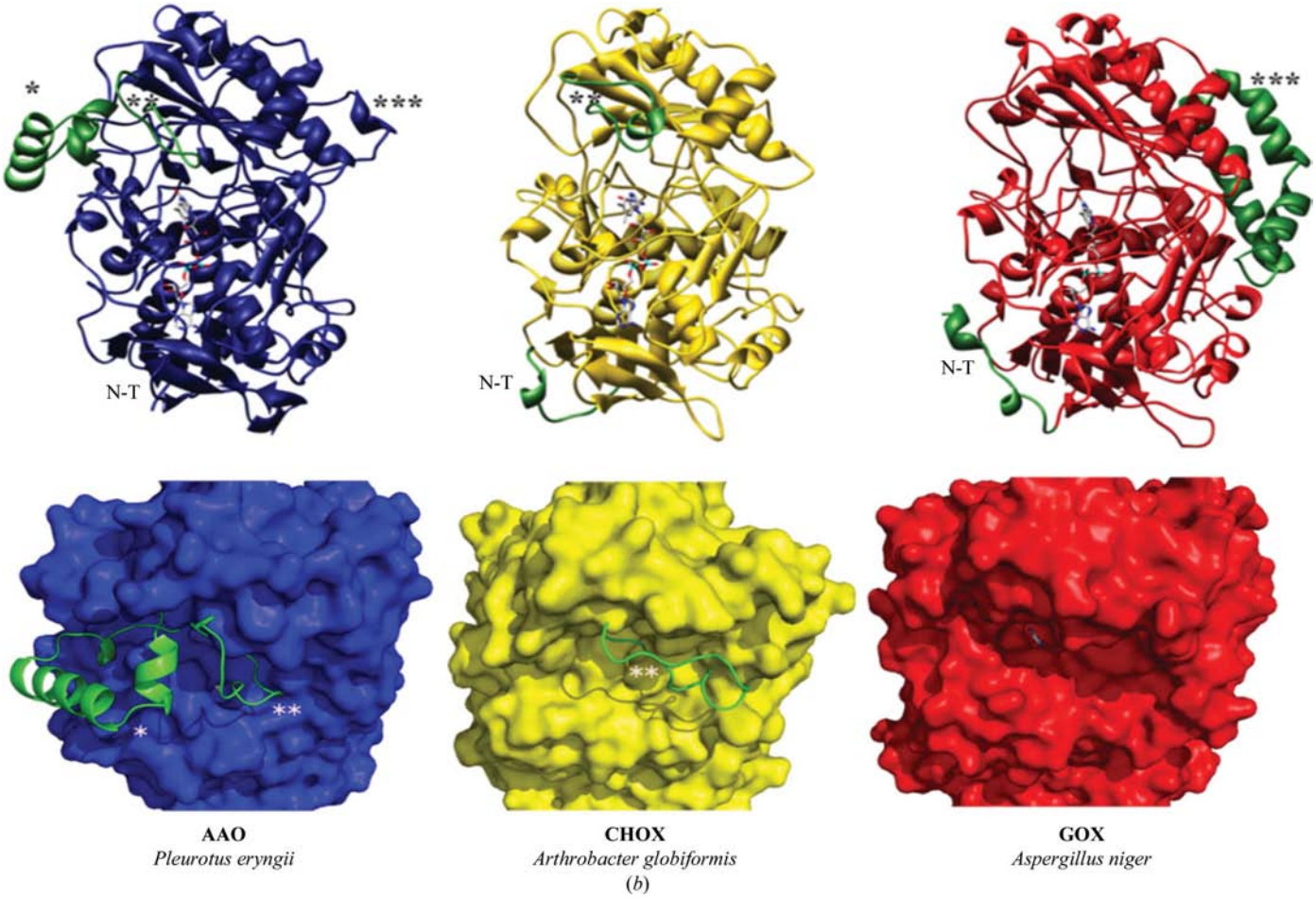

Figure 2 (continued)
(*b*) Top row: AAO, CHOX and GOX structures in the same orientation, depicted as ribbons with the FAD molecule as sticks. The differences in the structural motifs marked in the sequence alignment are shown in green. The FAD molecule is represented as sticks coloured according to atom type. Bottom row: FAD N^5 atom accessibility from bulk solvent in AAO, CHOX and GOX. The proteins are represented as coloured molecular surfaces, except for the additional structural elements, which are represented as green ribbons.

is thought to be related to the access of the substrate to the active site, as discussed below.

3.4. Substrate-access channel

The short insertion in the AAO sequence (shared with CHOX) and the extra structural motif in AAO (labelled * and **, respectively, in Fig. 2) establish an additional connection between the FAD-binding domain and the substrate-binding domain, creating a kind of flap just above the methyl groups of the isoalloxazine ring of FAD. These novel topological features in AAO generate a funnel-like channel that extends to the above-mentioned inner cavity along the *re* face of the cofactor's isoalloxazine ring (Fig. 4). This is in contrast to that observed in GOX (Hecht *et al.*, 1993), in which the absence of the extra motifs results in a wide opening providing access to the cofactor in the enzyme monomer (Fig. 2*b*). Wide access to the cofactor N^5 atom can also be observed in the monomer of pyranose-2-oxidase from *Phanerochaete chrysosporium* (Hallberg *et al.*, 2002), but the substrate-access channel in both carbohydrate oxidases is finally limited by the formation of multimeric complexes.

Therefore, the inner cavity in which the putative active site is located in AAO is only accessible through a narrow channel that is lined by residues Tyr92, Phe397 and Phe501 (Fig. 4), together with Val54, Pro55, His91, Pro79 and Val90. The lateral side chains of the first three aromatic residues define a highly hydrophobic bottleneck that blocks free access to the narrow inner cavity from the wide solvent-exposed cavity (Fig. 4). The internal cavity is flanked by the isoalloxazine ring of FAD on one side and by the highly conserved His502 and His546 that are involved in AAO catalysis (Varela *et al.*, 2000; Ferreira *et al.*, 2006) on the other. Interestingly, a water molecule is placed in this region, establishing hydrogen-bond interactions with both the N^5 atom of the isoalloxazine ring and the $N^{\varepsilon 2}$ atom of His502 (Fig. 5). Another feature in the surroundings of the isoalloxazine ring is the position adopted by the lateral chain of Glu389, which is close enough to His546 to interfere with its protonation state or to stabilize a transient positively charged form (Fig. 5).

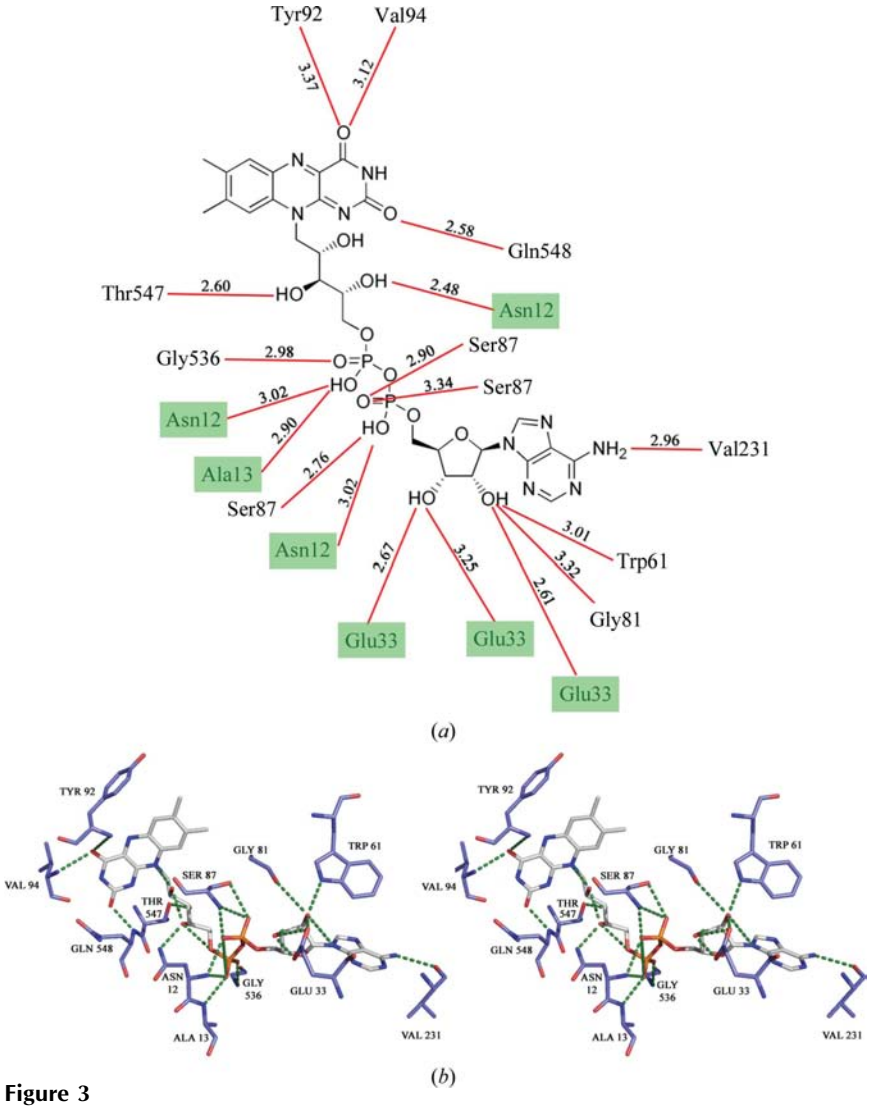

Figure 3
AAO–FAD interactions. (*a*) Schematic diagram of the AAO–FAD interactions. Hydrogen bonds are indicated by red lines, with the interatomic distances shown in Å. The residues that belong to the N-terminal DBM are indicated by green boxes. (*b*) Stereoview of the AAO–FAD interactions. The FAD molecule as well as the residues of AAO implicated in the interaction with FAD are depicted as sticks coloured according to atom type, with the C atoms of FAD in grey and those of the protein residues in blue. Hydrogen bonds are depicted as dashed green lines.

3.5. The active site of AAO: implications for substrate binding and electron transfer

Based on previous biochemical and molecular-modelling studies (Varela *et al.*, 2000; Ferreira *et al.*, 2006), it was proposed that the catalytic mechanism of AAO would involve electrophilic attack on the alcohol substrate assisted by a histidine residue located in the surroundings of the N^5 atom of the FAD flavin ring. His502 and His546 of AAO are both located in the vicinity of the inner cavity described previously and could act as general bases for the hydride-transfer reaction. This model might explain the lack of evidence for a stable semiquinone anionic radical intermediate and the evolutionary conservation of the histidine residues in the primary sequences of AAO and other GMC proteins. This mechanism is compatible with the structural data derived from the present model of AAO, in which an inner cavity near the catalytic histidines and the N^5 atom of FAD could accommodate the specific alcohol substrates. The lateral side chains of both histidines are situated close to the FAD

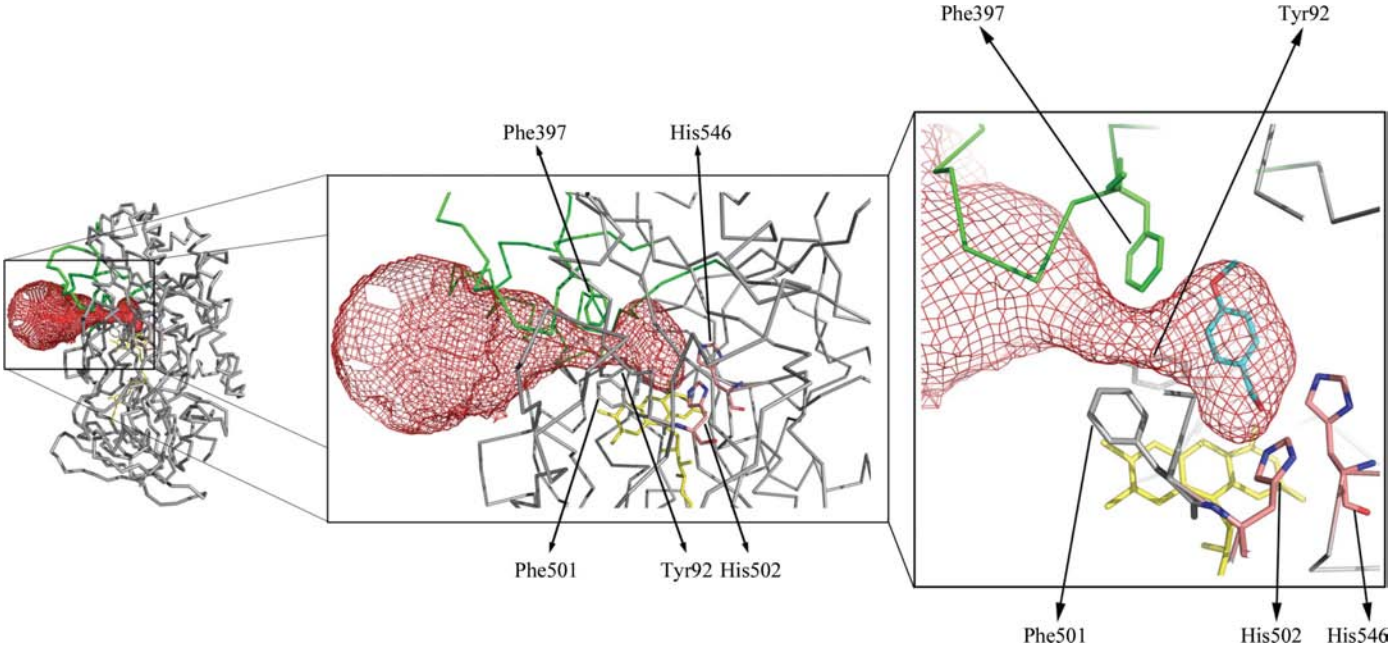

Figure 4
Substrate-access channel in AAO. The funnel-like hydrophobic channel connects the solvent with the putative active site through a bottleneck formed by three aromatic residues. The channel protrudes into an inner cavity between the isoalloxazine ring of FAD and the two catalytic histidines thought to be involved in substrate oxidation. The protein is represented as a grey backbone cartoon with the residues belonging to the additional structural motif of AAO in green. The FAD molecule is depicted as yellow sticks. The accessibility surface was calculated with *CAVER* (Petrek *et al.*, 2006) and is depicted as a red mesh. Right, docked model of the *p*-anisyl alcohol–AAO interaction; the alcohol molecule is situated in the inner cavity and depicted as sticks.

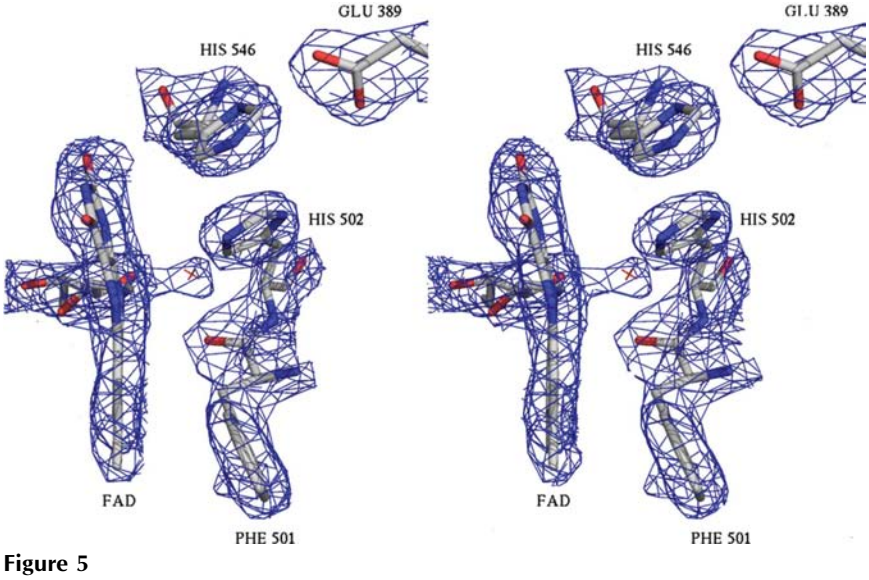

Figure 5
Active site of AAO. Top stereoview of the active-site residues and the isoalloxazine ring of FAD in AAO. The protein residues are represented as sticks coloured according to the atom type and inserted in a $2mF_c - DF_o$ experimental density map contoured at 1.5σ.

isoalloxazine ring and their $N^{\varepsilon 2}$ atoms are at distances that are compatible with their involvement in catalysis (Fig. 5). This finding is in agreement with the strong loss of activity of AAO variants in which these two residues were removed by site-directed mutagenesis (Ferreira *et al.*, 2006).

In order to gain insight into the catalytic mechanism of AAO, cocrystallization and soaking experiments were performed with known AAO substrates and inhibitors (Ferreira *et al.*, 2005). Unfortunately, low occupancy and/or a lack of ligand density prevented reasonable models of any complex from being built. To partially resolve this problem, a docking model of the preferred substrate of AAO, *p*-anisyl alcohol, was built (Fig. 4, right). A similar approach was used to localize reducing substrates at the active site of GOX and the flavin domain of cellobiose dehydrogenase (Hallberg *et al.*, 2002; Wohlfahrt *et al.*, 1999). The AAO alcohol substrate was docked in the inner cavity observed in the vicinity of the N^5 atom of the isoalloxazine ring of FAD and the catalytic histidines. In this position, *p*-anisyl alcohol places its C^{α} atom at a distance and angle (with respect to the flavin ring) similar to those described for other flavoenzymes (Fraaije & Mattevi, 2000). This position is compatible with a catalytic mechanism involving hydride transfer to the flavin N^5 atom aided by His502 (and His546) acting as catalytic base(s) for alcohol activation.

As mentioned above, direct access from the solvent to the active site is obstructed by three hydrophobic residues (Tyr92, Phe397 and Phe501), which produce a bottleneck that blocks free access of AAO alcohol substrates to this cavity (Fig. 4). Two of these residues (Tyr92 and Phe501) have been studied previously by site-directed mutagenesis, proving that they are essential for catalysis (Ferreira *et al.*, 2006). The two residues

are interchangeable, with no decrease in substrate affinity or catalytic efficiency, whereas substitution with a non-aromatic residue resulted in an inactive variant, stressing the importance of the aromatic character of the entrance to the active-site inner cavity that could establish interactions with the aromatic rings of the AAO substrates. The third residue that gives rise to the hydrophobic bottleneck, Phe397, has not yet been studied owing to the unexpected architecture of AAO, which was not inferred from previous modelling studies (Varela *et al.*, 2000). The implication of the lateral hydrophobic chain from this residue in closing the catalytic cavity suggests a fundamental role in regulating the access of the substrates to be oxidized by AAO.

4. Conclusions

Flavoenzymes have been implicated in a large number of biological processes (Decolibus & Mattevi, 2006) ranging from processes related to energy production to DNA repair or light emission (Joosten & van Berkel, 2007). Despite this broad spectrum of activities, flavoenzymes can be grouped into relatively few classes on the basis of their biochemical and structural properties (Dym & Eisenberg, 2001). The GMC family of oxidoreductases is characterized by the conservation of a core backbone of residues that define the interaction with FAD (Cavener, 1992). Although the core backbone shared by the whole family defines the interaction with the cofactor, no functional conservation has been linked to this observation; indeed, a high degree of variability in the chemical reactions catalyzed by these enzymes can be found (Dym & Eisenberg, 2001). The ability of flavoenzymes to oxidize different classes of chemical compounds demonstrates this variability.

Two different fungal oxidases, AAO and VAO, are involved in the oxidation of benzylic alcohols including lignin-derived products and related fungal metabolites. These two oxidases are paradigms for the functional diversity of flavoenzymes since they perform related molecular tasks through different catalytic mechanisms. While hydride transfer in VAO is promoted by the stabilization of a phenolate form of the substrate as a quinone methide (Mattevi *et al.*, 1997), AAO appears to make use of a conserved histidine residue as general base to promote the hydride-transfer reaction. This latter mechanism is similar to that described for other GMC oxidoreductases, which also involves the alkoxide form of the substrate (Gadda, 2008).

Different flavoenzymes, such as GOX, pyranose-2-oxidase and VAO, shield the residues implicated in catalysis from the solvent region by forming supramolecular complexes (Hecht *et al.*, 1993; Mattevi *et al.*, 1997; Hallberg *et al.*, 2002), while AAO behaves as a monomer (Guillen *et al.*, 1992). This characteristic is most probably related to its involvement in the extracellular degradation of lignin, since oligomeric ensembles would be more unstable under these conditions. However, AAO has developed an alternative way to 'bury' the active site based on the presence of two novel structural elements that fold over the isoalloxazine moiety of the FAD molecule. This structural limitation of the active-site access serves a dual role in AAO. On one hand, it is necessary owing to the hydrophobic nature of the substrates to be oxidized. On the other, it imposes steric constraints on the substrates that can reach the active site, since the access is limited by a narrow hydrophobic channel. The shape of this channel is modulated by the novel structural elements that, in this way, may fulfil a role in selecting the substrates able to reach the active site of AAO.

We would like to thank María Jesús Mate and Miguel Ortiz-Lombardía for discussion and comments on this manuscript. We acknowledge the support of the staff at the BW7A beamline station at DESY (Hamburg, Germany) and the BM16 beamline at ESRF (Grenoble, France). We are grateful to C. Fernández-Cabrera for excellent technical assistance. This work was supported by the Spanish grants BFU2008-02595, P-BIO-0214-2006 (BIPEDD-CM), BIO2005-03569, BIO2008-01522 and the BIORENEW project of the EU (contract NMP2-CT-2006-026456).

References

Aalten, D. M. van, Bywater, R., Findlay, J. B., Hendlich, M., Hooft, R. W. & Vriend, G. (1996). *J. Comput. Aided Mol. Des.* **10**, 255–262.
Baldrian, P. & Valaskova, V. (2008). *FEMS Microbiol. Rev.* **32**, 501–521.
Bannwarth, M., Bastian, S., Heckmann-Pohl, D., Giffhorn, F. & Schulz, G. E. (2004). *Biochemistry*, **43**, 11683–11690.
Camarero, S., Galletti, G. C. & Martinez, A. T. (1994). *Appl. Environ. Microbiol.* **60**, 4509–4516.
Carugo, O. & Djinovic Carugo, K. (2005). *Trends Biochem. Sci.* **30**, 213–219.
Cavener, D. R. (1992). *J. Mol. Biol.* **223**, 811–814.
Chen, L., Lyubimov, A. Y., Brammer, L., Vrielink, A. & Sampson, N. S. (2008). *Biochemistry*, **47**, 5368–5377.
Collaborative Computational Project, Number 4 (1994). *Acta Cryst.* D**50**, 760–763.
Cowtan, K. D. & Zhang, K. Y. (1999). *Prog. Biophys. Mol. Biol.* **72**, 245–270.
Davis, I. W., Leaver-Fay, A., Chen, V. B., Block, J. N., Kapral, G. J., Wang, X., Murray, L. W., Arendall, W. B. III, Snoeyink, J., Richardson, J. S. & Richardson, D. C. (2007). *Nucleic Acids Res.* **35**, W375–W383.
Decolibus, L. & Mattevi, A. (2006). *Curr. Opin. Struct. Biol.* **16**, 722–728.
DeLano, W. L. (2002). *The PyMOL Molecular Graphics System.* http://www.pymol.org.
Dym, O. & Eisenberg, D. (2001). *Protein Sci.* **10**, 1712–1728.
Emsley, P. & Cowtan, K. (2004). *Acta Cryst.* D**60**, 2126–2132.
Evans, C. S., Dutton, M. V., Guillén, F. & Veness, R. G. (1994). *FEMS Microbiol. Rev.* **13**, 235–239.
Evans, P. (2006). *Acta Cryst.* D**62**, 72–82.
Ferreira, P., Medina, M., Guillen, F., Martinez, M. J., Van Berkel, W. J. & Martinez, A. T. (2005). *Biochem. J.* **389**, 731–738.
Ferreira, P., Ruiz-Dueñas, F. J., Martinez, M. J., van Berkel, W. J. & Martinez, A. T. (2006). *FEBS J.* **273**, 4878–4888.
Fraaije, M. W. & Mattevi, A. (2000). *Trends Biochem. Sci.* **25**, 126–132.
Gadda, G. (2008). *Biochemistry*, **47**, 13745–13753.
Gouet, P., Courcelle, E., Stuart, D. I. & Métoz, F. (1999). *Bioinformatics*, **15**, 305–308.
Guillen, F. & Evans, C. S. (1994). *Appl. Environ. Microbiol.* **60**, 2811–2817.

Guillen, F., Martinez, A. T. & Martinez, M. J. (1992). *Eur. J. Biochem.* **209**, 603–611.
Gutierrez, A., Caramelo, L., Prieto, A., Martinez, M. J. & Martinez, A. T. (1994). *Appl. Environ. Microbiol.* **60**, 1783–1788.
Hallberg, B. M., Henriksson, G., Pettersson, G. & Divne, C. (2002). *J. Mol. Biol.* **315**, 421–434.
Hecht, H.-J., Kalisz, H. M., Hendle, J., Schmid, R. D. & Schomburg, D. (1993). *J. Mol. Biol.* **229**, 153–172.
Higuchi, T. (1997). *Biochemistry and Molecular Biology of Wood.* Berlin: Springer-Verlag.
Holm, L. & Sander, C. (1996). *Science*, **273**, 595–603.
Joosten, V. & van Berkel, W. J. (2007). *Curr. Opin. Chem. Biol.* **11**, 195–202.
Kirk, T. K. & Farrell, R. L. (1987). *Annu. Rev. Microbiol.* **41**, 465–505.
Langer, G., Cohen, S. X., Lamzin, V. S. & Perrakis, A. (2008). *Nature Protoc.* **3**, 1171–1179.
Lario, P. I., Sampson, N. & Vrielink, A. (2003). *J. Mol. Biol.* **326**, 1635–1650.
Laskowski, R. A., Moss, D. S. & Thornton, J. M. (1993). *J. Mol. Biol.* **231**, 1049–1067.
Leslie, A. G. W. (2006). *Acta Cryst.* D**62**, 48–57.
Lyubimov, A. Y., Heard, K., Tang, H., Sampson, N. S. & Vrielink, A. (2007). *Protein Sci.* **16**, 2647–2656.
Martinez, A. T., Rencoret, J., Marques, G., Gutierrez, A., Ibarra, D., Jimenez-Barbero, J. & del Rio, J. C. (2008). *Phytochemistry*, **69**, 2831–2843.
Martinez, A. T., Speranza, M., Ruiz-Dueñas, F. J., Ferreira, P., Camarero, S., Guillen, F., Martinez, M. J., Gutierrez, A. & del Rio, J. C. (2005). *Int. Microbiol.* **8**, 195–204.
Mathews, F. S., Chen, Z. W., Bellamy, H. D. & McIntire, W. S. (1991). *Biochemistry*, **30**, 238–247.
Mattevi, A. (2006). *Trends Biochem. Sci.* **31**, 276–283.
Mattevi, A., Fraaije, M. W., Mozzarelli, A., Olivi, L., Coda, A. & van Berkel, W. J. (1997). *Structure*, **5**, 907–920.
Muñoz, C., Guillén, F., Martínez, A. T. & Martínez, M. J. (1997). *Appl. Environ. Microbiol.* **63**, 2166–2174.
Murshudov, G. N., Vagin, A. A. & Dodson, E. J. (1997). *Acta Cryst.* D**53**, 240–255.
Pape, T. & Schneider, T. R. (2004). *J. Appl. Cryst.* **37**, 843–844.
Petrek, M., Otyepka, M., Banas, P., Kosinova, P., Koca, J. & Damborsky, J. (2006). *BMC Bioinformatics*, **7**, 316.
Pettersen, E. F., Goddard, T. D., Huang, C. C., Couch, G. S., Greenblatt, D. M., Meng, E. C. & Ferrin, T. E. (2004). *J. Comput. Chem.* **25**, 1605–1612.
Quaye, O., Lountos, G. T., Fan, F., Orville, A. M. & Gadda, G. (2008). *Biochemistry*, **47**, 243–256.
Ralph, J., Lundquist, K., Brunow, G., Lu, F., Kim, H., Schatz, P. F., Marita, J. M., Hatfield, R. D., Ralph, S. A., Christensen, J. H. & Boerjan, W. (2004). *Phytochem. Rev.* **3**, 29–60.
Ruiz-Dueñas, F. J., Ferreira, P., Martinez, M. J. & Martinez, A. T. (2006). *Protein Expr. Purif.* **45**, 191–199.
Ruiz-Dueñas, F. J., Morales, M., Garcia, E., Miki, Y., Martinez, M. J. & Martinez, A. T. (2009). *J. Exp. Bot.* **60**, 441–452.
Sheldrick, G. M. (2008). *Acta Cryst.* A**64**, 112–122.
Van Duyne, G. D., Standaert, R. F., Karplus, P. A., Schreiber, S. L. & Clardy, J. (1993). *J. Mol. Biol.* **229**, 105–124.
Varela, E., Martinez, M. J. & Martinez, A. T. (2000). *Biochim. Biophys. Acta*, **1481**, 202–208.
Varela, E., Martinez, A. T. & Martinez, M. J. (1999). *Biochem. J.* **341**, 113–117.
Winn, M. D., Murshudov, G. N. & Papiz, M. Z. (2003). *Methods Enzymol.* **374**, 300–321.
Wohlfahrt, G., Witt, S., Hendle, J., Schomburg, D., Kalisz, H. M. & Hecht, H.-J. (1999). *Acta Cryst.* D**55**, 969–977.